The self-sustained current oscillation and the dynamics in superlattices under the action of electric and magnetic fields

Gui Yang,[a] Hao Meng, Ling-Feng Zhang, and Shi-Ping Zhou[b]
Department of Physics, Shanghai University, 99 Shangda Road, Shanghai 200444, People's Republic of China

(Received 1 March 2008; accepted 15 April 2008; published online 16 June 2008)

Self-sustained time-dependent current oscillations have been found in weakly coupled GaAs/AlAs superlattices when the sequential resonant tunneling between adjacent quantum wells is the main electron transport mechanism. The oscillation regime was tunable by varying the doping densities and applied dc voltages. Based on the discrete sequential tunneling model, we theoretically studied the magnetic field dependence of the oscillation. The magnetic field B seems to be favorable for the formation of the static electric-field domains and to depress the current oscillation. Thus, the oscillation regime will be narrowed as the magnetic field strength increases. Driven by a transverse external microwave excitation, the system shows interesting nonlinear behaviors like quasiperiodicity, frequency locking, and periodicity. © *2008 American Institute of Physics*.
[DOI: 10.1063/1.2943264]

I. INTRODUCTION

Nonlinear vertical electron transport in negative differential velocity (NDV) in weakly coupled narrow-miniband semiconductor superlattices (SLs) results in the formation of electric-field domains (EFDs), which have been studied both experimentally[1–4] and theoretically.[5–10] It has been shown that when the main charge transport mechanism is sequential resonant tunneling between adjacent quantum wells, the NDV may lead to either stable self-sustained current oscillations[5,8,11] (SSCOs) or a sawtoothlike multistable current-voltage (I-V) characteristic.[1,2,6,12] The origin of the SSCO is related to the motion and recycling of electric field and charge domain walls over a few periods of the SL while the sawtoothlike I-V characteristics are associated with the formation of the static EFDs.[1] These behaviors then crucially depend on the SL configuration (widths of wells and barriers, number of SL periods, and boundary conditions in the contact regions),[13] the doping density,[14] the voltage bias, and the sample temperature.[15–17] Recently, the influence of a transverse magnetic field (B) on the current-voltage characteristics has been investigated.[1,3,8,10] It is possible to tune the tunneling processes from stable field domains to unstable field domains (current oscillations) in a SL. In other words, the SSCO regime will be modified by applying magnetic fields. However, up to now, there has not been a detailed theoretical analysis about magnetic field dependence of the SSCO and of the EFD as well.

In this paper, we adopt a discrete sequential tunneling model[7] to study the weakly coupled GaAs/AlAs SL under the crossed electric field and the magnetic field B up to 20 T. We theoretically show that the drift velocity of electrons driven by an electric field will be modified by a transverse magnetic field. Thus, the NDV region is altered with B and thereby the SSCO. As illustrated in Fig. 2(a), in the absence of external magnetic field, the SSCOs can exist in a weakly coupled GaAs/AlAs SL only when it was appropriately doped and biased, i.e., in a certain range of the doping level λ and the bias voltage U_{dc}. Outside the range, either a buildup of stable EFDs at higher carrier concentration or a state of almost uniform electric field distribution at lower carrier concentrations is observed. The effect of a transverse external magnetic field B seems to be favorable for the formation of the stable EFDs due to the localization of the tunneling electrons under the action of the Lorentz force. Indeed, the SSCO area reduces in the $(U_{dc}-\lambda)$ plane accompanied by a certain shift to higher bias voltages with increasing B. Besides, the response of the SSCO to the microwave excitation is also studied. Due to the competition between the intrinsic oscillation and the external ac signal, the system displays different modes, including the periodicity, frequency locking, and quasiperiodicity. The corresponding Poincaré mapping, phase portraits, and the first return map are presented to help understand the nonlinear effects.

II. THE MODEL AND THE NDV REGION FOR ELECTRON TRANSPORT IN SL

Consider a system consisting of N quantum wells under an electric field perpendicular to the layers, i.e., along the z direction. Therefore, the intensities of the tunneling current are determined by electrons tunneling from the ground states E_1^{i-1} in the $(i-1)$th well to the ground states $(E_1^{i-1}-E_1^i)$, the first excited states $(E_1^{i-1}-E_2^i)$, and the second excited states $(E_1^{i-1}-E_3^i)$ of the ith well. In a transverse magnetic field parallel to the x axis the electron tunneling from well to well, separated by distance l of the SL period, picks up the transverse momentum $\hbar k_y = eBl$ due to the Lorentz force. This results in an energy transferring $\Delta E = e^2B^2l^2/(2m^*)$ from the z direction to the y direction. To maintain the resonant condition this energy has to be compensated by means of, e.g., an electric field of $\Delta F = \Delta E/(\mathrm{el})$. The calculated electron drift

[a]Electronic mail: kuiziyang@shu.edu.cn.
[b]Author to whom correspondence should be addressed. Electronic mail: spzhou@shu.edu.cn.

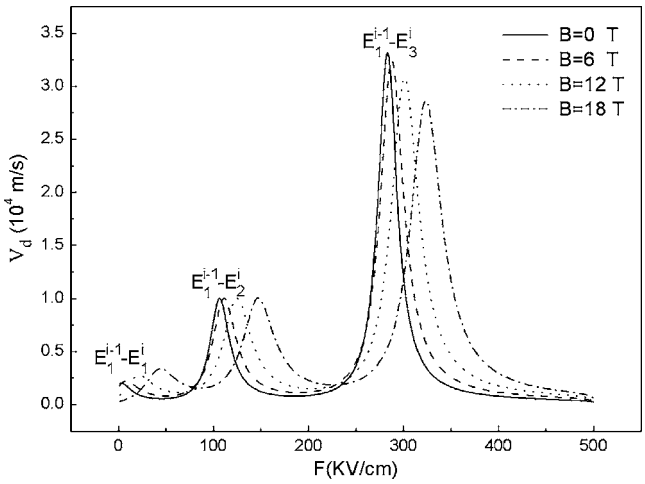

FIG. 1. Calculated electron drift velocity as a function of the electric field at the magnetic field $B=0$, 6, 12, and 18 T.

velocity as a function of the electric field[1] is shown in Fig. 1. The solid, dash, dot, and dash-dot lines represent the curves for $B=0$, 6, 12, and 18 T, respectively. Clearly, the peak velocity locations that correspond to the occurrence of resonant tunneling of electrons shift to higher electric fields with the increase in magnetic fields B.

The dynamics of the system can be described by the average electric field $F_i(t)$ and the electron density $n_i(t)$ in the ith well. These variables are governed by the discrete Poisson equations, the Ampere's law, and the voltage bias conditions as follows:

$$\frac{1}{l}(F_i - F_{i-1}) = \frac{e}{\varepsilon}(n_i - N_D), \tag{1}$$

$$\varepsilon \frac{dF_i}{dt} + en_i v_d(F_i) = J(t), \tag{2}$$

$$l\sum_{i=1}^{N} F_i = U(t), \tag{3}$$

$$\varepsilon(F_i - F_0)/(\mathrm{el}) = n_1 - N_D = \delta N_D. \tag{4}$$

In these Eqs. (4) is the boundary condition at the first contact, and $i=1,2,\ldots,N$ is the well index. ε, e, and N_D are the permittivity, electron charge, and doping density, respectively. The total current density $J(t)$ is the sum of the displacement current and the electron flux via a series of sequential resonant tunneling. The total applied voltage $U(t)$ in Eq. (3) can be written as $U(t)=U_{\mathrm{dc}}\{1+A\sin(2\pi f_d t)\}$, where

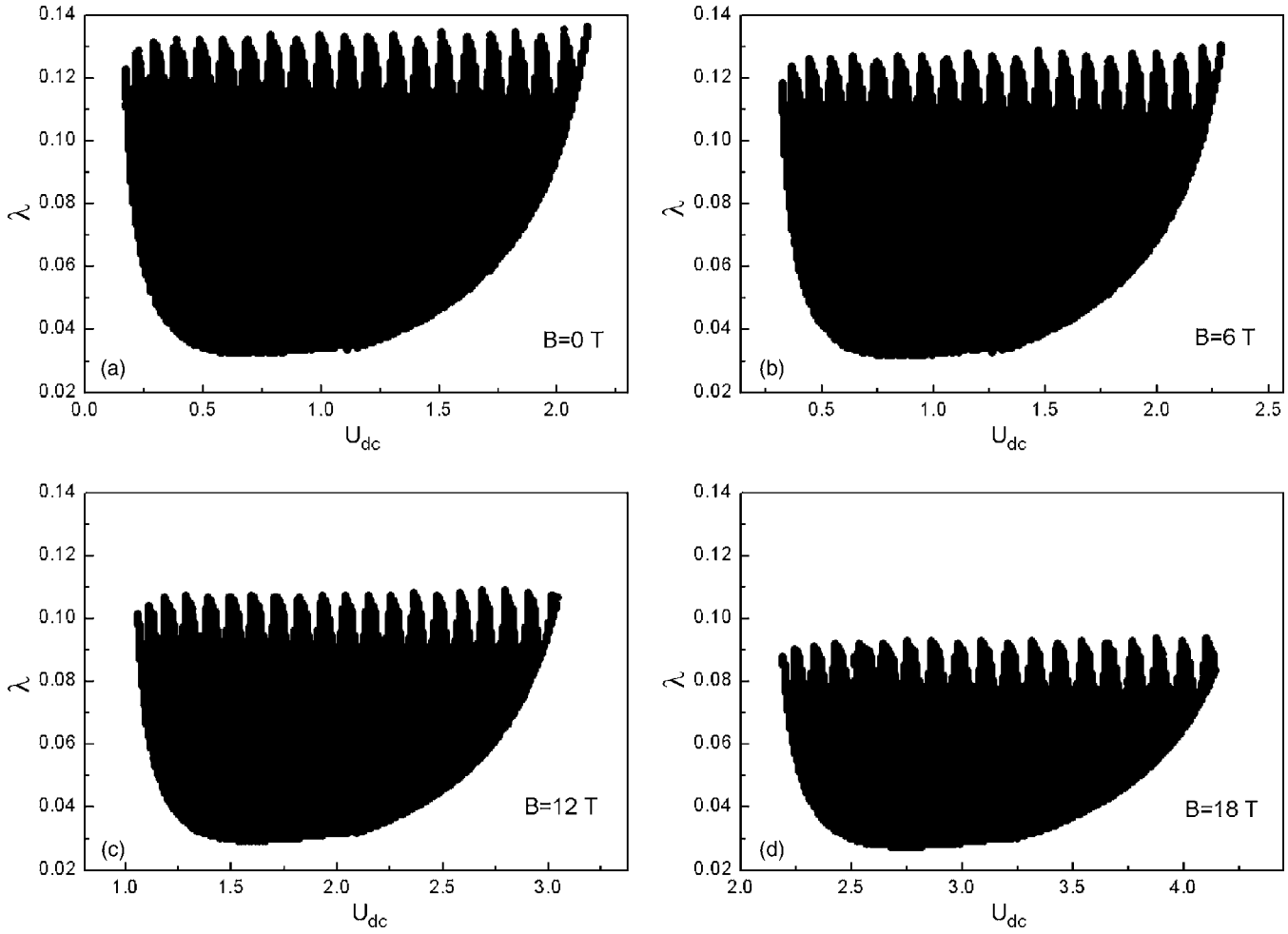

FIG. 2. The phase diagram in the applied voltage and the doping density ($U_{\mathrm{dc}}-\lambda$) plane for (a) $B=0$ T, (b) $B=6$ T, (c) $B=12$ T, and (d) $B=18$ T. Here λ is in units of n_0 and U_{dc} is in units of volt. The system inside the shadowed area will have a SSCO solution.

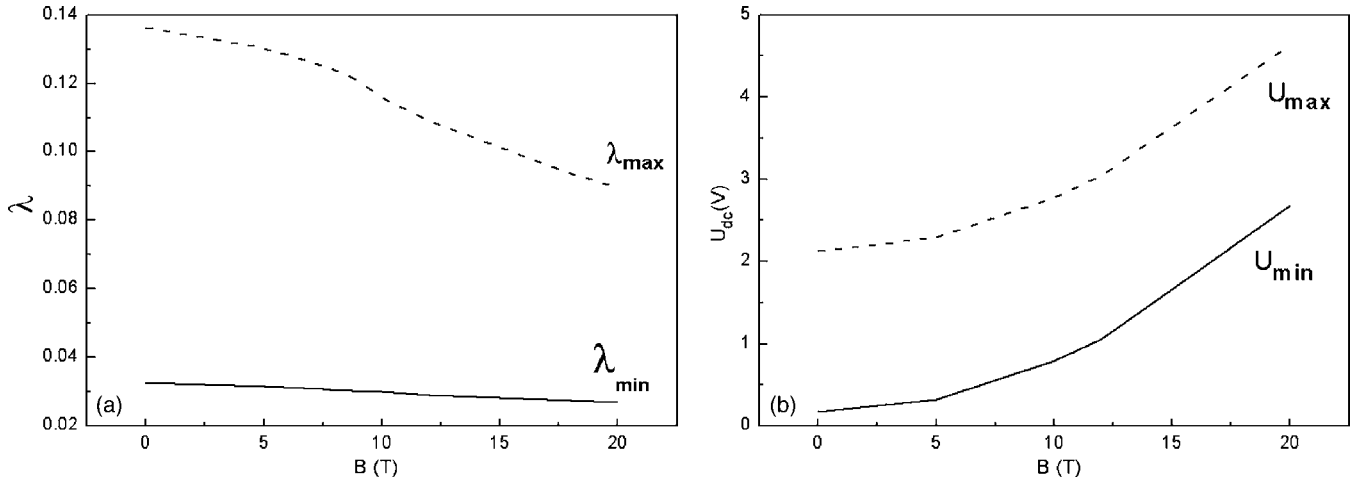

FIG. 3. The lower and the upper boundaries for (a) the doping density λ and (b) the applied voltage U_{dc} as a function of the magnetic field B in the existence of the SSCO.

U_{dc} is the dc voltage and A and f_d are the relative amplitude and driving frequency of an ac microwave signal.

In our numerical simulations, we use the dimensionless variables: $\Phi_i = F_i/F_{1-2}$, $F_{1-2} = (E_2^i - E_1^{i-1})/(\text{el})$, $n_0 = \varepsilon F_{1-2}/(\text{el})$, $\lambda = N_D/n_0$, $t_{\text{tun}} = l/v_d(F_{1-2})$, $\tau = t/t_{\text{tun}}$, $w = 2\pi f_d t_{\text{tun}}$, $V = U_{dc}/(F_{1-2}lN)$, and $a = AV$. The dimensionless equations for the electric field read

$$\frac{d\Phi_i}{d\tau} = \frac{1}{N}\sum_{j=1}^{N} v_d(\Phi_j)[\Phi_j - \Phi_{j-1} + \lambda] - v_d(\Phi_i)[\Phi_i - \Phi_{i-1} + \lambda] + aw\cos(w\tau). \quad (5)$$

With Eq. (4) and the initial condition $\Phi_i(0) = V$, we solve Eqs. (5) by the fourth order Runge–Kutta method.

III. THE SSCO WITH TRANSVERSE MAGNETIC FIELDS

Firstly, we discuss how SSCO varies with the control parameter: the doping density and the dc voltage. As an example, we consider a weakly GaAs/AlAs(n-doped/undoped) SL,[13] which consists of 40 periods of 9.0 nm GaAs well and 4.0 nm AlAs barrier with the ground state energy $E_1 = 44$ meV, the first excited state $E_2 = 180$ meV, the second excited state $E_3 = 410$ meV, etc. The lattice temperature is maintained at $T = 5$ K. Referring to Fig. 1, we see that there are three NDV regions corresponding to $(E_1^{i-1} - E_1^i)$, $(E_1^{i-1} - E_2^i)$, and $(E_1^{i-1} - E_3^i)$, which means that the SSCOs are excepted as the dc voltage is biased within these regions. We focus on the first NDV region in this paper. For the pure dc case ($a = 0$), the SLs exhibit an undamped time-periodic SSCO when the doping density and the dc bias are between some critical values. In Figs. 2(a)–2(d), we plot the phase diagram of the SSCO regime in the applied voltage and the doping density ($U_{dc} - \lambda$) plane for various B values, where λ and the bias U_{dc} are in units of n_0 and volt, respectively. The shadowed areas correspond to possible SSCO regimes where the system will have a SSCO solution. In the absence of external magnetic field, i.e., $B = 0$ T, when the doping density λ is in the range (0.032 55, 0.136 25) and the dc bias is within (0.1728, 2.1276), the SSCO exists, which is similar to the phase diagram of Sun *et al.*[18] Increasing B to 6 T, the boundary of the doping density becomes between 0.0317 and 0.1303 while the bias changes from 0.324 to 2.2896. Increasing B further up to 12 T, the SSCO can be observed in the

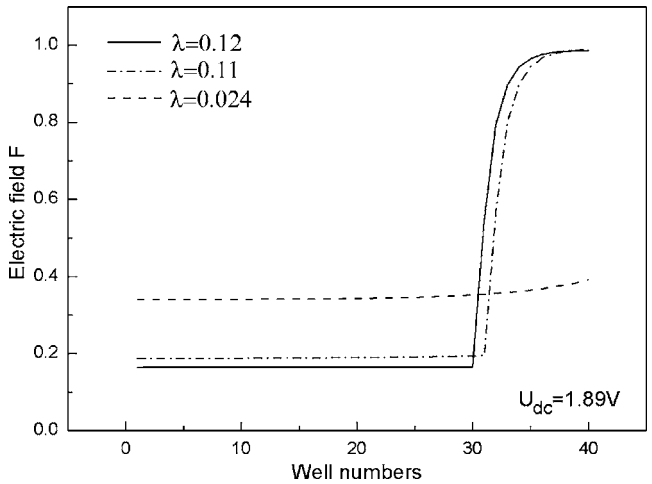

FIG. 4. The electric field profile for the doping density λ is above or below the SSCO regime at $B = 12$ T and the dc voltage $U_{dc} = 1.89$ V.

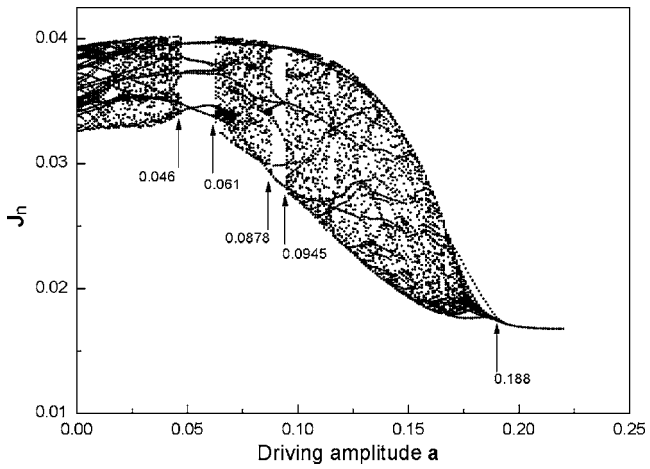

FIG. 5. The Poincaré bifurcation diagram of the current density J_n vs the driving amplitude a at $B = 12$ T.

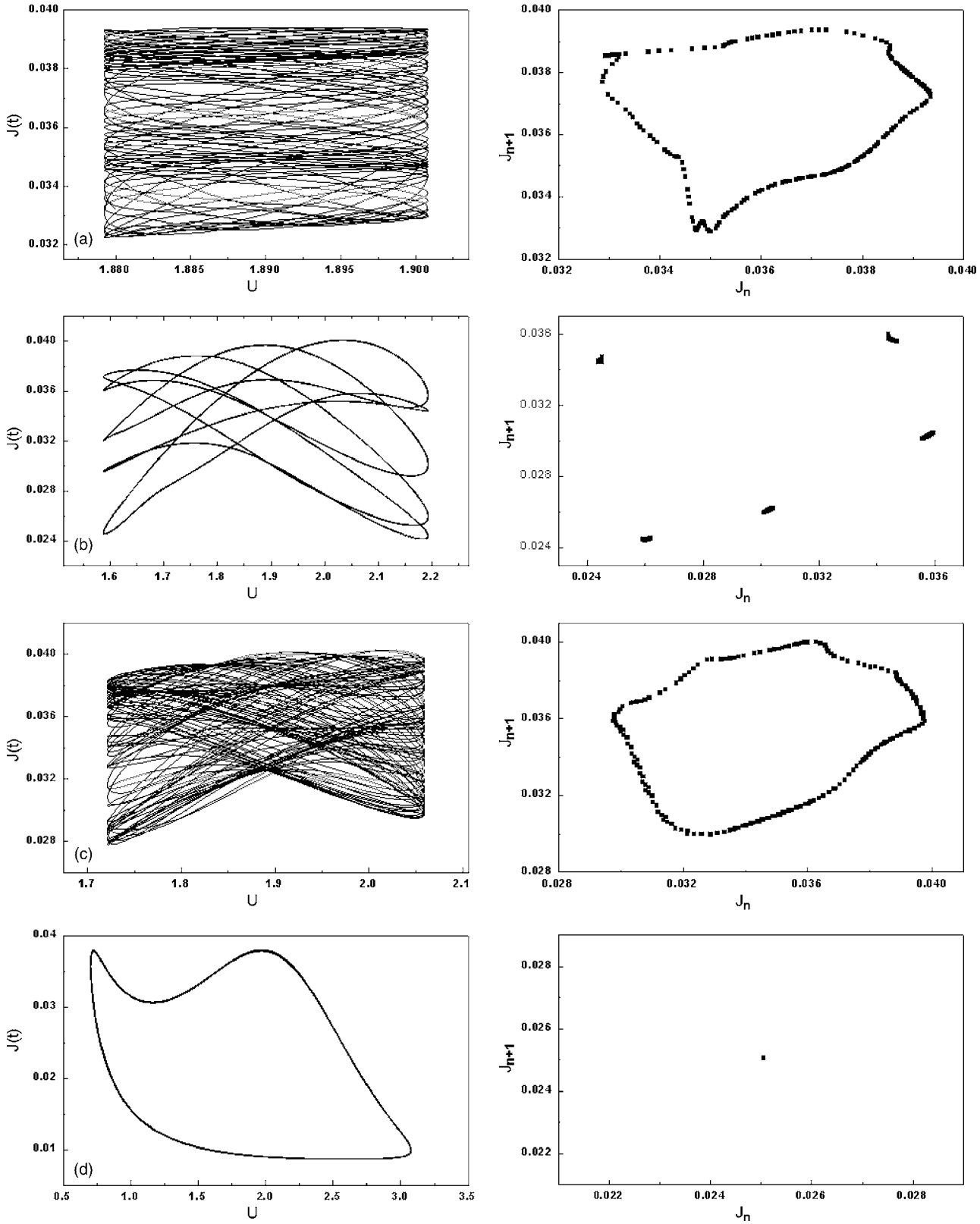

FIG. 6. Phase portraits (left) and the corresponding first return map (right) for different amplitudes *a* (a) 0.002 (quasiperiodicity), (b) 0.0562 (period-5), (c) 0.0676 (quasiperiodicity), and (d) 0.21 (period-1).

region of $\lambda \in (0.0291, 0.109)$ and $U_{dc} \in (1.0584, 3.0456)$. As for $B=18$ T, the SSCO requires that $\lambda \in (0.0274, 0.0937)$ and $U_{dc} \in (1.0584, 3.0456)$. One then notices that the SSCO regime has been steadily squeezed by increasing magnetic field B. To make the process clearer, we plot the diagram of λ and U_{dc} versus the magnetic field B in Figs. 3(a) and 3(b), where, λ_{max}, λ_{min}, U_{max}, and U_{min} denote the maximum and minimum of the doping density and dc voltage values in the SSCO regime for each magnetic field B. Figure 3(a) shows that both λ_{max} and λ_{min} will drop with increasing B, but λ_{max}

decreases more rapidly than λ_{min}. Thus, the value of the difference between λ_{max} and λ_{min} will be smaller. In Fig. 3(b), U_{max} and U_{min} increase simultaneously with increasing B. However, the value of the difference $(U_{max}-U_{min})$ is almost unchanged. Therefore, the change in the SSCO regime is mainly caused by the variety of the doping density range. This can be understood as follows. The formation of stationary EFDs is possible for a sufficient high doping density.[17] Due to the tunneling electrons under the action of the Lorentz force, the magnetic field helps to form the stationary EFDs in SL. For a higher doping density close to the λ_{max} in the SSCO regime, the transition between SSCOs and the stable EFDs occur and λ_{max} will be less with increasing B. As for a lower doping density near λ_{min}, it is insufficient to form the stationary EFDs under the applied magnetic field. Thus, there exists almost no change in the lower boundary, as shown in Fig. 3(a). Consequently, the SSCO regime will be smaller for a higher magnetic field B, which makes sense to speak of the depression of SSCOs and the formation of the stable high field domain associated with the external magnetic fields.

In addition, we found that the electric field profile is different when the doping density is above and below the SSCO range. We choose $B=12$ T as an example. As shown in Fig. 4, the stable EFD corresponds to the higher carrier density while the state of almost uniform electric field distribution is at a lower carrier density. In Fig. 4, the two domains of the low electric field (LEF) and the high electric field (HEF) are separated by a domain boundary in the form of a charge accumulation layer (CAL) in SL. A larger doping density will more easily to form the stationary CAL, which means that the transition from LEF to HEF will be earlier for a high doping density than for a low doping level, as illustrated in Fig. 4.

IV. NONLINEAR DYNAMICS WITH THE DRIVING MICROWAVE SIGNAL

When the SL structure is subject to an ac voltage in the presence of magnetic fields, a variety of nonlinear spatiotemporal behaviors are expected. We choose the dc voltage $U_{dc}=1.89$ V, the doping density $\lambda=0.07$, and the magnetic field $B=12$ T, and the SSCO is then found with frequency $f_0=8.9$ MHz. In this section, we shall consider the ac driving amplitude $a \in (0.0, 0.22)$ as the control parameter by fixing the driving frequency $f_d=mf_0$ [where $m=(\sqrt{5}+1)/2 \approx 1.618\,03\ldots$ is the inverse golden mean ratio], and we calculate the current density J in the time domain.

To detect and visualize the current oscillation modes, we plot the Poincaré mapping in the current density versus the ac amplitude space. Let $T_d=1/f_d$ be the driving period. We sample the current density J_n at times $T_n=nT_d$, $n=1,2,\ldots$ (after waiting enough time for the transients to have decayed out). For each ac amplitude a we compute $J_n=J(nT_d)$ until the solution becomes stable within a 10^{-5} accuracy. At that time, we stop the simulation and depict all the J_n corresponding to one period of the solution. The corresponding Poincaré bifurcation diagram is plotted in Fig. 5. Thus, aperiodic solutions can be very easily distinguished from periodic ones by the number of points in Poincaré mapping orbit as the ac amplitude varies. In the case of $0<a<0.046$, the system exhibits aperiodic oscillation modes. Period-5 and period-6 oscillations can be found in the range of $0.046 \leqslant a < 0.061$. With further increasing a to the range of $0.061 \leqslant a < 0.0878$, aperiodic oscillation modes reappear. For $0.0878 \leqslant a < 0.0945$, period-5 and period-8 occur. Corresponding to $a \in (0.0945, 0.188)$, it is the aperiodic solution. When the driving amplitude $a \geqslant 0.188$, the period-1 oscillations exist and the spatiotemporal solution of the system is synchronized with the driving signal. To have a deep insight into the transition between different dynamic states, we plot the current-voltage phase portrait and the corresponding first return map in Fig. 6. The left plots and the right plots indicate the I-V phase portraits and the first return map for different driving amplitudes: (a), $a=0.002$, (b) 0.0562 (b), (c), 0.0676 and (d) 0.21. The phase portrait for a period-n solution appears as simple closed loops and n separate points in the first return map. Therefore, Figs. 6(b) and 6(d) indicate the periodic-5 and periodic-1 orbits, respectively. As for the aperiodic phase portrait, the corresponding first return map will be more complicated. For the quasiperiodic orbits, the first return map looks like a closed loop. So, the oscillation orbits in Figs. 6(a) and 6(c) are quasiperiodicity.

V. CONCLUSIONS

We theoretically investigate the effect of external magnetic fields on SSCOs in a weakly coupled GaAs/AlAs SLs when the system is driven by a single dc voltage. The diagram of the SSCO regime is plotted in a voltage-doping density plane. We show that the magnetic field favors the formation of the stationary EFDs by depressing the established SSCOs under the dc bias. Therefore, the regime where SSCO occurs will decrease with increasing magnetic field, as shown in Fig. 2. We show also that the electric field profiles in the SL are different for various doping densities, with other control parameters unchanged. In addition, the response of the SSCO to the external driving signal is studied. As a result of the coupling between the intrinsically generated periodic motion of the accumulated charge wave and an external driving signal, the system will operate in different modes depending on the driving ac signal amplitude.

ACKNOWLEDGMENTS

This work was supported by the National Natural Science Foundation of China under Grant No. 60671042 and by Science and Technology Committee of Shanghai Municipal for key research projects (Grant No. 06JC14032).

[1] B. Q. Sun, J. N. Wang, W. K. Ge, Y. Q. Wang, D. S. Jiang, H. J. Zhu, H. L. Wang, Y. M. Deng, and S. L. Feng, Phys. Rev. B **60**, 8866 (1999).
[2] M. Rogozia, S. W. Teitsworth, H. T. Grahn, and K. H. Ploog, Phys. Rev. B **65**, 205303 (2002).
[3] B. Q. Sun, J. N. Wang, and D. S. Jiang, Semicond. Sci. Technol. **20**, 947 (2005).
[4] Z. Z. Sun, Y. Sun, X. R. Wang, J. P. Cao, Y. P. Wang, and Y. Q. Wang, Appl. Phys. Lett. **87**, 182110 (2005).
[5] M. Zwolak, D. Ferguson, and M. DiVentra, Phys. Rev. B **67**, 081303 (2003).
[6] L. L. Bonilla, R. Escobedo, and G. Dell'Acqua, Phys. Rev. B **73**, 115341

(2006).
[7]L. L. Bonilla, J. Phys.: Condens. Matter **14**, R341 (2002).
[8]C. Wang and J. C. Cao, Chaos **15**, 013111 (2005).
[9]Z. Z. Sun, H. T. He, J. N. Wang, S. D. Wang, and X. R. Wang, Phys. Rev. B **69**, 045315 (2004).
[10]X. R. Wang and Q. Niu, Phys. Rev. B **59**, R12755 (1999).
[11]A. Amann, A. Wacker, and E. Schöll, Physica B **314**, 404 (2002).
[12]R. Aguado, G. Platero, M. Moscoso, and L. L. Bonilla, Phys. Rev. B **55**, R16053 (1997).
[13]J. Kastrup, R. Hey, K. H. Ploog, H. T. Grahn, L. L. Bonilla, M. Kindelan, M. Moscoso, A. Wacker, and J. Galán, Phys. Rev. B **55**, 2476 (1997).
[14]A. Wacker, M. Moscoso, M. Kindelan, and L. L. Bonilla, Phys. Rev. B **55**, 2466 (1997).
[15]D. Sánchez, L. L. Bonilla, and G. Platero, Phys. Rev. B **64**, 115311 (2001).
[16]C. Y. Li, B. Q. Sun, D. S. Jiang, and J. N. Wang, Semicond. Sci. Technol. **16**, 239 (2001).
[17]X. R. Wang, J. N. Wang, B. Q. Sun, and D. S. Jiang, Phys. Rev. B **61**, 7261 (2000).
[18]Z. Z. Sun, K. L. Chen, S. Yin, H. T. He, J. N. Wang, Y. Q. Wang, and X. R. Wang, New J. Phys. **6**, 148 (2004).